



Noise Suppression Using Symmetric Exchange Gates in Spin Qubits

Frederico Martins,¹ Filip K. Malinowski,¹ Peter D. Nissen,¹ Edwin Barnes,^{2,3} Saeed Fallahi,⁴ Geoffrey C. Gardner,⁵
Michael J. Manfra,^{4,5,6} Charles M. Marcus,¹ and Ferdinand Kuemmeth^{1,*}

¹*Center for Quantum Devices, Niels Bohr Institute, University of Copenhagen, 2100 Copenhagen, Denmark*

²*Department of Physics, Virginia Tech, Blacksburg, Virginia 24061, USA*

³*Condensed Matter Theory Center and Joint Quantum Institute, Department of Physics, University of Maryland, College Park, Maryland 20742-4111, USA*

⁴*Department of Physics and Astronomy and Birck Nanotechnology Center, Purdue University, West Lafayette, Indiana 47907, USA*

⁵*School of Materials Engineering and Birck Nanotechnology Center, Purdue University, West Lafayette, Indiana 47907, USA*

⁶*School of Electrical and Computer Engineering, Purdue University, West Lafayette, Indiana 47907, USA*

(Received 23 November 2015; published 16 March 2016)

We demonstrate a substantial improvement in the spin-exchange gate using symmetric control instead of conventional detuning in GaAs spin qubits, up to a factor of six increase in the quality factor of the gate. For symmetric operation, nanosecond voltage pulses are applied to the barrier that controls the interdot potential between quantum dots, modulating the exchange interaction while maintaining symmetry between the dots. Excellent agreement is found with a model that separately includes electrical and nuclear noise sources for both detuning and symmetric gating schemes. Unlike exchange control via detuning, the decoherence of symmetric exchange rotations is dominated by rotation-axis fluctuations due to nuclear field noise rather than direct exchange noise.

DOI: 10.1103/PhysRevLett.116.116801

Spin qubits, basic units of quantum information built from the spin states of electrons in solid-state systems, are one of the most promising realizations of a qubit [1]. This is due to their potential for miniaturization, scalability, and fault tolerance [2,3]. In fact, experiments in recent years have demonstrated remarkable progress in the coherent manipulation of single- and multispin devices [4–7]. Nevertheless, one of the main difficulties with spin qubits, and more generally with solid-state qubits, is the decoherence due to interactions with the environment. In the case of electron spins confined in semiconductor quantum dots, two main types of environmental noise limit coherence: electrical noise and hyperfine interactions with nuclear spins in the surrounding lattice [8–10]. To reach the high control fidelities necessary for quantum computing, the coupling between a quantum dot spin qubit and its environment can be reduced by the use of sweet spots [11–13], and pulse errors can be reduced by bootstrap tomography [14,15].

A crucial component of any spin-based quantum computing platform is strong spin-spin interaction. In their seminal article, Loss and DiVincenzo proposed that exchange interactions between electron spins could be controlled by the height of the tunnel barrier between neighboring quantum dots [16]. However, until recently this proposal was not implemented in the laboratory, and instead exchange interactions were induced by raising or lowering the potential of one dot relative to the other, an approach referred to as tilt or detuning control [17]. Unlike the dot-symmetric tunnel barrier control method, tilt control affects the two dots asymmetrically and hybridizes the (1,1) and (0,2) charge states. Here numbers within each

parenthesis denote occupation number of the left dot and right dot. In Fig. 1(a) we illustrate the difference between the two methods. First, a singlet state $(0,2)S$ is prepared (P). Thereafter, the electrons are adiabatically separated to the $|\uparrow\downarrow\rangle$ state in the (1,1) charge configuration. At the exchange point (X), a pulse is performed. For the tilt case, during this pulse the wave functions of the electrons are brought together by asymmetrically deforming the confining potential of the dots. In the case of the symmetric mode of operation, the exchange interaction is increased by lowering the potential barrier between the two dots. Finally, reversing the slow adiabatic passage first projects the final two-spin state onto $|\uparrow\downarrow\rangle$ and then maps it onto $(0,2)S$, which is then read out at the measurement point (M).

In this Letter, we demonstrate rapid, high-quality exchange oscillations implemented by pulsing the barrier between two dots, as envisioned in the original Loss-DiVincenzo proposal. We also show that, unlike tilt-induced qubit rotations, the coherence of barrier-induced rotations is not limited by electrical detuning noise, but rather by nuclear spin fluctuations parallel to the applied magnetic field. We quantify the improvements by studying exchange oscillations within a singlet-triplet qubit, corresponding to $\sqrt{\text{SWAP}}$ operations between the two spins. Alternatively, benchmarking of single-qubit gate fidelities is in principle possible but requires nuclear programming [4]. Recent work on surface acoustic waves and silicon triple quantum dots showed results consistent with some of our observations [18,19], indicating that symmetric exchange finds applications beyond GaAs qubits.

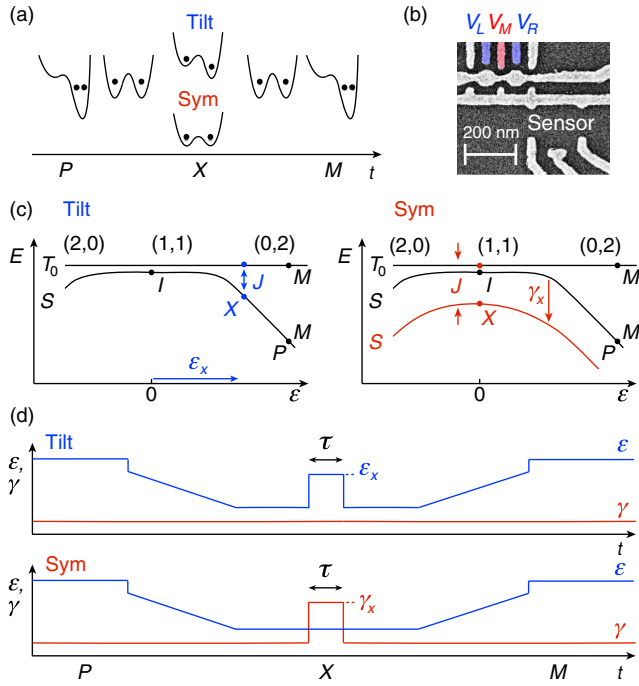


FIG. 1. (a) Schematic comparison of detuning (tilt) and symmetric exchange pulse sequences, showing double-dot potentials and dot occupancies. Tilt, wave function overlap controlled by detuning the confining potential. Symmetric, wave function overlap controlled by lowering the potential barrier between dots. (b) Electron micrograph of the device consisting of a double dot and charge sensor. Note the gate that runs through the center of the dots. A 10 nm HfO_2 layer is deposited below the gates to allow positive and negative gating. High-bandwidth lines are connected to left and right plungers gates V_L , V_R (blue), and the middle barrier gate V_M (red). (c) Energy diagrams of the two-electron spin singlet, S , and spin-zero triplet, T_0 , as a function of detuning ϵ . (Left) Tilt mode, exchange J is controlled by detuning ϵ , set by V_L and V_R . (Right) Symmetric mode, J is controlled interdot coupling γ set by V_M (red curve). (d) Pulse sequences for tilt and symmetric modes, with amplitudes ϵ_x and γ_x during the exchange pulse, respectively.

The double quantum dot device with integrated charge sensor [20] is shown in Fig. 1(b). The device was fabricated on a GaAs/AlGaAs heterostructure 57 nm below the surface, producing a two-dimensional electron gas with bulk density $n = 2.5 \times 10^{15} \text{ m}^{-2}$ and mobility $\mu = 230 \text{ m}^2/\text{Vs}$. To minimize stray capacitance a mesa was patterned using electron-beam lithography and wet etching. Metallic gates (Ti/Au) were deposited after atomic layer deposition of 10 nm HfO_2 , which allows both positive and negative gating, and obviates gate-bias cooling [21]. All measurements were conducted in a dilution refrigerator with mixing chamber temperature below 50 mK and in-plane magnetic field $B = 300 \text{ mT}$ applied perpendicular to the axis between dots.

Voltage pulses were applied via high-bandwidth coaxial lines to the left and right plunger gates, V_L , V_R , and the barrier between the dots, V_M . In practice, to account for the

small coupling asymmetries, all three gates are involved in applying detuning ϵ and symmetric barrier control γ :

$$\begin{aligned} \epsilon &= k_0[(V_R - V_R^0) - (V_L - V_L^0)] + k_1(V_M - V_M^0), \\ \gamma &= V_M - V_M^0, \end{aligned} \quad (1)$$

where V_R^0 , V_L^0 , and V_M^0 are dc offset voltages (see Supplemental Material [22]). Parameters $k_0 = 0.5$ and $k_1 = -0.075$ were determined experimentally by mapping out the charge stability diagram. The value of k_0 is consistent with previous experiments and sets the difference between left and right dot electrochemical potential, whereas k_1 keeps other charge states energetically unaccessible during γ pulses.

Energy levels for the two-electron singlet S and triplet T_0 states as a function of detuning ϵ are shown in Fig. 1(c), along with the pulse sequences for the tilt and symmetric operation modes in Fig. 1(d). For both tilt and symmetric operation, two electrons are prepared (P) in a singlet $(0,2)S$ state and, by slowly ramping ϵ to $(1,1)$, the system is initialized (I) into the ground state of the nuclear Overhauser field, either $|\uparrow\downarrow\rangle$ or $|\downarrow\uparrow\rangle$. For tilt operation, the exchange pulse J is applied by detuning to the exchange (X) point ϵ_x for a duration τ , inducing rotations between $|\uparrow\downarrow\rangle$ and $|\downarrow\uparrow\rangle$. For symmetric operation, the exchange pulse is applied by pulsing the middle gate to γ_x .

Two-dimensional images of exchange oscillations, controlled by either tilt [Fig. 2(a)] or symmetric operation near the midpoint of $(1,1)$ [Fig. 2(b)], show a striking difference in quality. In both images, each pixel represents the singlet return probability, P_S , measured from an ensemble of $\sim 10^3$ single-shot measurements. Each single-shot measurement is assigned a binary value by comparing the reflectometer signal at the measurement (M) point, integrated for $T_M = 10 \mu\text{s}$, to a fixed threshold [20,24]. Figure 2(c) shows exchange oscillations using both tilt and exchange. This image is generated by applying a tilt pulse of amplitude ϵ_x (of either sign) along with a fixed symmetric pulse $\gamma_x = 190 \text{ mV}$ for a duration τ . As $|\epsilon_x|$ is increased J also increases, producing a chevronlike pattern centered around the sweet spot $J(\epsilon_x = 0)$ that occurs in the middle of the $(1,1)$ charge state. Defining a quality factor Q to be the number of oscillations before the amplitude decays to $1/e$ of its initial value, we measure $Q \sim 35$ at the symmetry point, $\epsilon_x = 0$ [25].

The oscillation frequency of $P_S(\tau)$ gives a direct measure of J at the exchange point X . Interestingly, the frequency does not depend on the Overhauser field, even when it is comparable in size to J [26]. Figures 3(a) and 3(b) show a set of experimental exchange oscillations representative of the tilt and symmetric operation mode, respectively. Q extracted from such oscillations is shown in the insets. Consistent with previous observations [17,27], tilt-induced exchange oscillations result in $Q \sim 6$ independent of J . On the other hand, for the symmetric mode, Q increases with J for the range measured of $40 \text{ MHz} < J < 700 \text{ MHz}$. This

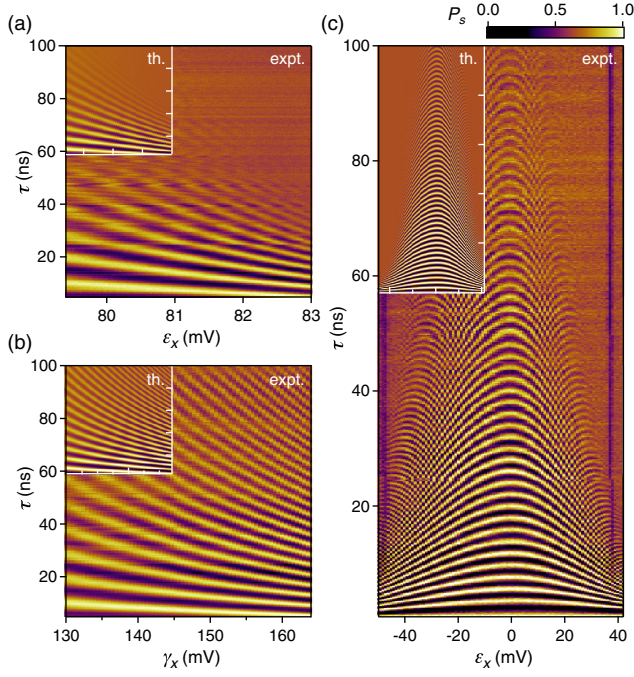


FIG. 2. (a) Probability of detecting a singlet P_s as a function of ϵ_x and exchange time τ for tilt-induced oscillations ($\gamma_x = 0$ mV). (b) P_s as a function of γ_x and exchange time τ obtained for barrier-induced oscillations near the symmetry point ($\epsilon_x = 13.5$ mV). (c) Same as (a) with barrier pulse activated, $\gamma_x = 190$ mV, revealing the sweet spot of the symmetric operation. The dark vertical features near 39 and -44 mV are due to leakage from the singlet state to the spin-polarized triplet state. Insets show theoretical simulations for each experimental situation.

is in agreement with recent results in singlet-triplet qubits fabricated in the Si/SiGe heterostructures [19]. Much higher values of Q can be obtained by tilting the double dot potential so far that both S and T_0 states share the same $(0,2)$ charge state [8]. However, it is unclear if qubit operations at frequencies of tens of GHz are practical.

To quantify the noise sensitivity of the symmetric exchange gate as well as gain insight into why it outperforms exchange by detuning, we compare both methods to a simple model that includes both nuclear Overhauser gradient noise and voltage noise on the detuning and barrier gates. Noise is assumed Gaussian and quasistatic on the time scale of the exchange oscillations. Nuclear noise is characterized by a mean longitudinal Overhauser gradient energy h_0 between dots, with standard deviation σ_h . Exchange noise is assumed to result from voltage noise on the left and right plungers and the barrier, with mean exchange energy J with standard deviation σ_J . The model also accounts for triplet-to-singlet relaxation at the measurement point, with a relaxation time T_{RM} during the measurement interval of length T_M . Within this model, the singlet return probability $\langle\langle P_s \rangle\rangle$ over both noise ensembles is given by [26]

$$\begin{aligned} \langle\langle P_s \rangle\rangle &= 1 - \frac{T_{RM}}{T_M} \left(1 - e^{-\frac{T_M}{T_{RM}}}\right) \frac{e^{-\frac{h_0^2}{2\sigma_h^2}} e^{-\frac{J^2}{2\sigma_J^2}}}{\sqrt{\pi}\sigma_h\sigma_J} \\ &\times \int_{-\pi/2}^{\pi/2} d\chi \left\{ \frac{b(\chi)}{a(\chi)^{3/2}} e^{\frac{b(\chi)^2}{a(\chi)}} \right. \\ &\left. - \text{Re} \left[\frac{b(\chi) + i\tau \sec(\chi)}{a(\chi)^{3/2}} e^{\frac{[b(\chi) + i\tau \sec(\chi)]^2}{a(\chi)}} \right] \right\}, \end{aligned} \quad (2)$$

where χ is the tilt of the qubit rotation axis during an exchange pulse due to the Overhauser field gradient [26], $a(\chi) \equiv 2\tan^2\chi/\sigma_h^2 + 2/\sigma_J^2$ and $b(\chi) \equiv h_0 \tan\chi/\sigma_h^2 + J/\sigma_J^2$.

The black solid lines in Fig. 3, together with the insets in Figs. 2(a), 2(b), and 2(c), are generated by evaluating Eq. (2) numerically. Two fit parameters per curve are the oscillation frequency J and a horizontal offset associated with the rise time of the waveform generator. All other parameters were obtained from independent measurements: The Overhauser energy gradient fluctuation, $\sigma_h = 23$ MHz, was obtained by measuring the distribution of free induction decay frequencies [9] over a 30 min interval and fitting the distribution to a Gaussian.

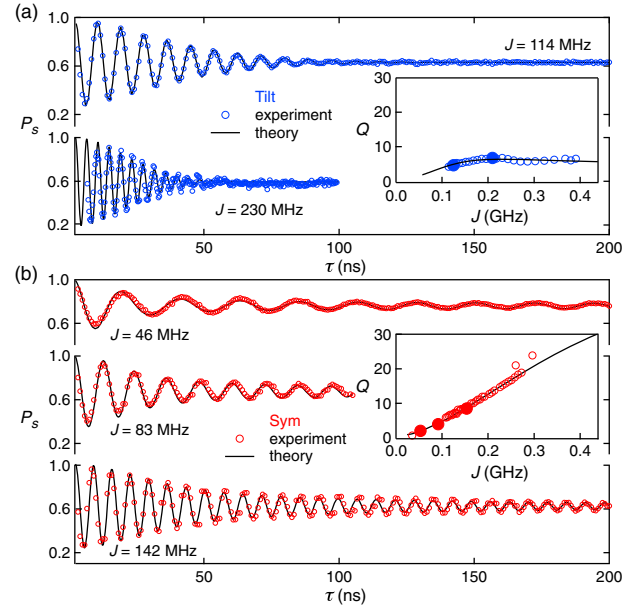


FIG. 3. (a) Tilt-induced exchange oscillations (i.e., $\gamma_x = 0$ mV) for $\epsilon_x = 79.5$ and 82 mV, generating oscillation frequencies indicated by J . (b) Same as (a) but for the symmetric mode of operation ($\epsilon_x = 13.5$ mV), with $\gamma_x = 100, 120,$ and 140 mV. Open circles are experimental data. Solid lines correspond to the theoretical model in Eq. (2), with J and a horizontal offset being the only adjustable parameters. Insets show the quality factor Q , defined as the number of oscillations before the amplitude damps by a factor of e , as a function of J for both tilt and symmetric operation modes. Solid circles correspond to data in the main panel, and solid lines are theoretical predictions.

The saturation of the singlet return probability P_S , at long τ , denoted P_{sat} , will deviate from $P_{\text{sat}} = 0.5$ in the presence of a nonzero mean Overhauser field gradient h_0 or finite relaxation time T_{RM} . Fitting the J dependence of P_{sat} [Fig. 4(a)], yields fit values $T_{RM} = 30 \mu\text{s}$ and $h_0/h = 40 \text{ MHz}$.

Exchange noise σ_J is obtained by assuming (i) all noise is gate noise, (ii) noise on different gates is independent: $\sigma_J^2 = \sigma_{\text{el}}^2 [(dJ/dV_L)^2 + (dJ/dV_M)^2 + (dJ/dV_R)^2]$. In giving all three components equal weight, we have further assumed that all three gates are equally noisy as quantified by the parameter σ_{el} . Taking into account the definitions in Eq. (1) we obtain

$$\sigma_J = \sigma_{\text{el}} \sqrt{2k_0^2 \left(\frac{dJ}{d\varepsilon_x} \right)^2 + \left(\frac{dJ}{d\gamma_x} + k_1 \frac{dJ}{d\varepsilon_x} \right)^2}. \quad (3)$$

The derivatives are calculated from a phenomenological smooth exchange profile $J(\varepsilon_x, \gamma_x)$ fitted to a discrete map of

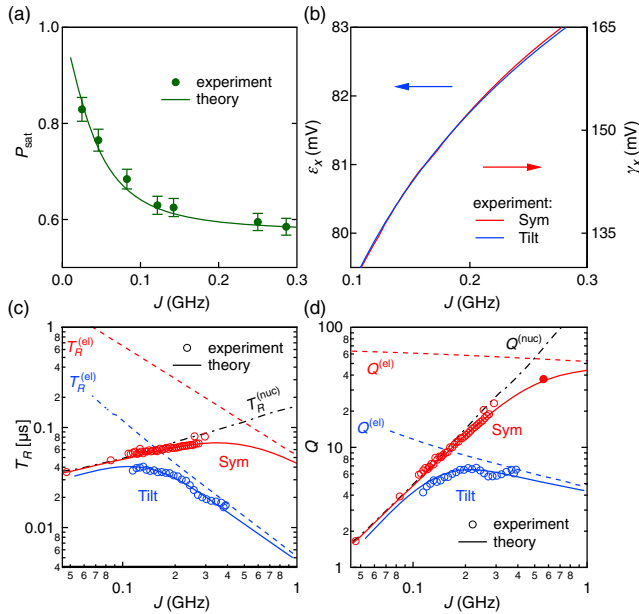


FIG. 4. (a) Saturation probability of the symmetric mode of operation P_{sat} as a function of J (symbols). Comparison with theory (solid line) determines T_{RM} and h_0 . (b) Plot of ε_x for the tilt and γ_x for the symmetric mode of operation, as functions of the exchange coupling extracted experimentally. (c) Decoherence time T_R , i.e., time before the amplitude of oscillations is reduced by a factor of e , as a function of J for both tilt and symmetric modes. (d) Quality of the exchange rotations, defined as $Q = JT_R$, for different J . In (c) and (d) the open circles are obtained experimentally and solid lines correspond to a model that includes dephasing due to electrical and nuclear noise. Black dashed lines are the same model if we only consider nuclear noise contributions ($T_R^{(\text{nuc})}$, $Q^{(\text{nuc})}$). Blue and red dashed lines correspond to the electrical noise contributions ($T_R^{(\text{el})}$, $Q^{(\text{el})}$) for the tilt and symmetric modes of operation, respectively. The solid circle indicates the maximum Q value observed in Fig. 2(c).

J measured at various operating points (see Supplemental Material [22]). The effective gate noise σ_{el} is extracted from tilt exchange oscillations measured in a regime where effective detuning noise dominates, giving $\sigma_{\text{el}} = 0.18 \text{ mV}$ (see Supplemental Material [22]). This value, together with Eq. (3), determines $\sigma_J(\varepsilon_x, \gamma_x)$ used in all simulations, and yields excellent agreement with data.

The origin of the improved electrical performance becomes apparent when comparing the required pulse amplitudes for symmetric and tilted operation for a given J [Fig. 4(b)]. Although the dependences of ε_x and γ_x on J are similar, the range of ε_x is significantly smaller than γ_x . Note in Fig. 4(b) that J changes from 0.1 to 0.3 GHz for a $\sim 3 \text{ mV}$ change in ε_x , or a $\sim 30 \text{ mV}$ change in γ_x [see Fig. 4(b)]. Because of this difference in derivatives of J with respect to ε_x and γ_x , the symmetric operation has much less noise for a given noise in the gate voltages.

The contributions of nuclear and electrical noise to limiting the quality factor Q of and dephasing time, $T_R = Q/J$, comparing experiment and model, is shown in Figs. 4(c) and 4(d). Note that for detuning (tilt) operation, electrical noise dominates above $\sim 0.2 \text{ GHz}$, so that going any faster (using larger J) just makes the exchange noise greater in proportion, limiting the number of oscillations to $Q \sim 6$. For symmetric exchange, on the other hand, electrical noise does not dominate until above $J \sim 0.6 \text{ GHz}$, resulting in a monotonically increasing quality factor up to $\sim 1 \text{ GHz}$. From the model, we find Q as high as 50, 8 times larger than in the conventional tilt operation mode. Finally, we note that the origin of the effective electrical noise may be within the sample and not in the instrumentation. To distinguish actual voltage fluctuations on the gate electrodes (due to instrumentation) from intrinsic noise source (e.g., two-phonon processes [28]), further studies, including temperature dependence are needed.

In summary, we have investigated experimentally and modeled the application of an exchange gate applied by opening the middle barrier at a symmetry point of a two-electron spin qubit system instead of the conventional method, which is to detune the potential. The model allows the influences of nuclear and electrical noise to be disentangled for both symmetric and detuning exchange control, and is in excellent agreement with experimental data. We find that the symmetric mode of control is significantly less sensitive to electrical noise due to the symmetric arrangement, making exchange only quadratically sensitive to detuning gate voltage noise. With this new symmetric control method, we were able to increase the quality factor of coherent oscillations from around 6 to 35, and expect that improvements beyond $Q \sim 50$ are possible by further increasing J . The corresponding enhancement of coherence times by nearly an order of magnitude will also benefit other single- and multiqubit implementations that rely on exchange interactions [29].

We thank Rasmus Eriksen for help in fast data acquisition and Daniel Loss and Mark S. Rudner for helpful discussions. This work was supported by IARPA-MQCO, LPS-MPO-CMTC, the EC FP7-ICT project SiSPIN No. 323841, the Army Research Office, and the Danish National Research Foundation.

F. M. and F. K. M. contributed equally to this work.

*Corresponding author.

kuemmeth@nbi.dk

- [1] C. Kloeffer and D. Loss, *Annu. Rev. Condens. Matter Phys.* **4**, 51 (2013).
- [2] J. M. Taylor, H.-A. Engel, W. Dür, A. Yacoby, C. M. Marcus, P. Zoller, and M. D. Lukin, *Nat. Phys.* **1**, 177 (2005).
- [3] D. D. Awschalom, L. C. Bassett, A. S. Dzurak, E. L. Hu, and J. R. Petta, *Science* **339**, 1174 (2013).
- [4] S. Foletti, H. Bluhm, D. Mahalu, V. Umansky, and A. Yacoby, *Nat. Phys.* **5**, 903 (2009).
- [5] H. Bluhm, S. Foletti, D. Mahalu, V. Umansky, and A. Yacoby, *Phys. Rev. Lett.* **105**, 216803 (2010).
- [6] J. R. Petta, H. Lu, and A. C. Gossard, *Science* **327**, 669 (2010).
- [7] M. D. Shulman, O. E. Dial, S. P. Harvey, H. Bluhm, V. Umansky, and A. Yacoby, *Science* **336**, 202 (2012).
- [8] O. E. Dial, M. D. Shulman, S. P. Harvey, H. Bluhm, V. Umansky, and A. Yacoby, *Phys. Rev. Lett.* **110**, 146804 (2013).
- [9] C. Barthel, J. Medford, H. Bluhm, A. Yacoby, C. M. Marcus, M. P. Hanson, and A. C. Gossard, *Phys. Rev. B* **85**, 035306 (2012).
- [10] H. Bluhm, S. Foletti, I. Neder, M. Rudner, D. Mahalu, V. Umansky, and A. Yacoby, *Nat. Phys.* **7**, 109 (2011).
- [11] C. H. Wong, M. A. Eriksson, S. N. Coppersmith, and M. Friesen, *Phys. Rev. B* **92**, 045403 (2015).
- [12] T. Hiltunen, H. Bluhm, S. Mehl, and A. Harju, *Phys. Rev. B* **91**, 075301 (2015).
- [13] J. Fei, J.-T. Hung, T. S. Koh, Y.-P. Shim, S. N. Coppersmith, X. Hu, and M. Friesen, *Phys. Rev. B* **91**, 205434 (2015).
- [14] V. V. Dobrovitski, G. de Lange, D. Riste, and R. Hanson, *Phys. Rev. Lett.* **105**, 077601 (2010).
- [15] P. Cerfontaine, T. Botzem, D. P. DiVincenzo, and H. Bluhm, *Phys. Rev. Lett.* **113**, 150501 (2014).
- [16] D. Loss and D. P. DiVincenzo, *Phys. Rev. A* **57**, 120 (1998).
- [17] J. R. Petta, A. C. Johnson, J. M. Taylor, E. A. Laird, A. Yacoby, M. D. Lukin, C. M. Marcus, M. P. Hanson, and A. C. Gossard, *Science* **309**, 2180 (2005).
- [18] B. Bertrand, H. Flentje, S. Takada, M. Yamamoto, S. Tarucha, A. Ludwig, A. D. Wieck, C. Bauerle, and T. Meunier, *Phys. Rev. Lett.* **115**, 096801 (2015).
- [19] M. D. Reed, B. M. Maune, R. W. Andrews, M. G. Borselli, K. Eng, M. P. Jura, A. A. Kiselev, T. D. Ladd, S. T. Merkel, I. Milosavljevic, E. J. Pritchett, M. T. Rakher, R. S. Ross, A. E. Schmitz, A. Smith, J. A. Wright, M. F. Gyure, and A. T. Hunter, this issue, *Phys. Rev. Lett.* **116**, 110402 (2016).
- [20] C. Barthel, D. J. Reilly, C. M. Marcus, M. P. Hanson, and A. C. Gossard, *Phys. Rev. Lett.* **103**, 160503 (2009).
- [21] C. Buizert, F. H. L. Koppens, M. Pioro-Ladrière, H.-P. Tranitz, I. T. Vink, S. Tarucha, W. Wegscheider, and L. M. K. Vandersypen, *Phys. Rev. Lett.* **101**, 226603 (2008).
- [22] See Supplemental Material at <http://link.aps.org/supplemental/10.1103/PhysRevLett.116.116801> for details about noise analysis, which includes Ref. [23].
- [23] D. J. Reilly, C. M. Marcus, M. P. Hanson, and A. C. Gossard, *Appl. Phys. Lett.* **91**, 162101 (2007).
- [24] C. Barthel, M. Kjaergaard, J. Medford, M. Stopa, C. M. Marcus, M. P. Hanson, and A. C. Gossard, *Phys. Rev. B* **81**, 161308R (2010).
- [25] Figure 2(c) shows that barrier-induced exchange oscillations have high quality factors for a wide range of operating points ϵ_x near the sweet spot. For example, data shown in Fig. 2(b) was obtained at $\epsilon_x = 13.5$ mV, which, for practical purposes, we also classify as symmetric operation.
- [26] E. Barnes, M. S. Rudner, F. Martins, F. K. Malinowski, C. M. Marcus, and F. Kuemmeth, *Phys. Rev. B* **93**, 121407(R) (2016).
- [27] A. P. Higginbotham, F. Kuemmeth, M. P. Hanson, A. C. Gossard, and C. M. Marcus, *Phys. Rev. Lett.* **112**, 026801 (2014).
- [28] V. Kornich, C. Kloeffer, and D. Loss, *Phys. Rev. B* **89**, 085410 (2014).
- [29] M. Veldhorst, C. H. Yang, J. C. C. Hwang, W. Huang, J. P. Dehollain, J. T. Muhonen, S. Simmons, A. Laucht, F. E. Hudson, K. M. Itoh, A. Morello, and A. S. Dzurak, *Nature (London)* **526**, 410 (2015).